An Investigation Into the Fast- and Slow-Scale Instabilities of a Single Phase Bidirectional Boost Converter

Sudip K. Mazumder, *Member, IEEE,* Ali H. Nayfeh, and Dushan Boroyevich, *Member, IEEE*

***Abstract*—We develop an analytical map for a single phase bidirectional boost converter. This map enables the analysis of the dynamics of the converter faster and without any convergence problems. For the closed-loop converter, we show how instabilities can occur on the slow and fast scales. Conventional analyzes based on averaged models can not predict the fast-scale instability because such models do not account for the switching-frequency ripple.**

***Index Terms*—Bifurcation, boost, converter, Poincare map, single phase.**

I. Introduction

SINGLE-PHASE converters are widely used in power electronics [1]–[10]. They are used in applications ranging from traction drives to telecommunications. One of the most common circuits used to achieve unity power factor is a time-varying single phase bidirectional boost converter (SPBBC) as shown in Fig. 1. A SPBBC has the capability to draw sinusoidal line currents at unity power factor, thereby significantly minimizing the total harmonic distortion of the line current. The operation of the converter has been analyzed by some researchers [1]–[3]. However, very few have even attempted to properly analyze the stability of such converters. The system of equations for an SPBBC involves discontinuity in control and is time-varying. As such, the analysis of SPBBC is difficult.

Some publications have analyzed the SPBBC or systems similar to it using smooth averaged models. Mohan *et al.* [1] used the concept of quasistatic analysis to analyze the current-loop stability of an SPBBC operating with hysteretic control. Williams [3] developed a small-signal model to facilitate the design of an output-voltage compensator for resistive and constant-power loads. Sanders *et al.* [11], proposed a more comprehensive approach to derive generalized averaged models of multi-phase converters. Recently, the dynamic phasor modeling technique has been used to analyze unbalanced multi-phase power systems [12]. This technique,

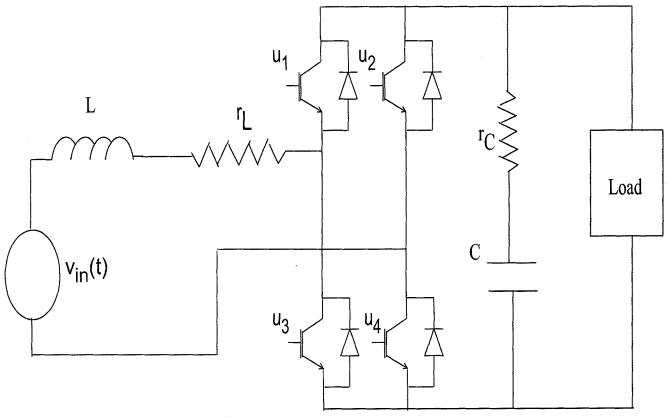

Fig. 1. Single-phase-bidirectional-boost converter.

which builds upon the generalized averaging method proposed by Sanders *et al.* [11], is a polyphase generalization of the dynamic phasor approach, and it is applicable to nonlinear power system models. In steady state, the dynamic phasors reduce to standard phasors from ac circuit theory. In an alternate approach, Jacobina *et al.* [13] have proposed the concept of a vector model to analyze the transient and steady-state behaviors of polyphase systems operating under balanced and unbalanced conditions.

These analyses have some shortcomings. The conventional averaged model completely neglects the impact of the switching frequency and hence cannot predict the dynamics on the fast scale. We have demonstrated in our earlier papers that instability in a standalone or an integrated converter can occur on a slow as well as on a fast scale [14]–[16]. Similar results have been published in [25]–[35] as well. Recently Bass and Sun [23] and Bass and Lehman [24] have extended the conventional averaging methodology by taking into account the effect of fast-scale dynamics. However, even such a model cannot describe chaotic dynamics. Even the slow-scale averaged model may have more than one equilibrium solution or more than one stable orbit. However, a linearized small-signal analysis ignores the presence of these other solutions. Therefore, a small-signal analysis can not predict anything about the domain of attraction of the nominal solution or orbit. For example, the averaged model of a multi-loop dc-dc boost converter may have a quadratic nonlinearity [17]. In other words, this system may have more than one equilibrium solution. If two of these solutions are stable, then the system will have two operating points, one of which

Manuscript received September 4, 2001; revised February 1, 2003. Recommended by Associate Editor B. Lehman.

S. K. Mazumder is with the Power Electronics Research Center, Department of Electrical and Computer Engineering, University of Illinois at Chicago, Chicago, IL 60616 USA (e-mail: mazumder@ece.uic.edu).

A. H. Nayfeh is with the Nonlinear Vibrations Laboratory, Department of Engineering Science and Mechanics, Virginia Polytechnic Institute and State University, Blacksburg, VA 24061 USA.

D. Boroyevich is with the Center for Power Electronics Systems, Department of Electrical and Computer Engineering, Virginia Polytechnic Institute and State University, Blacksburg, VA 24061 USA.

Digital Object Identifier 10.1109/TPEL.2003.813769

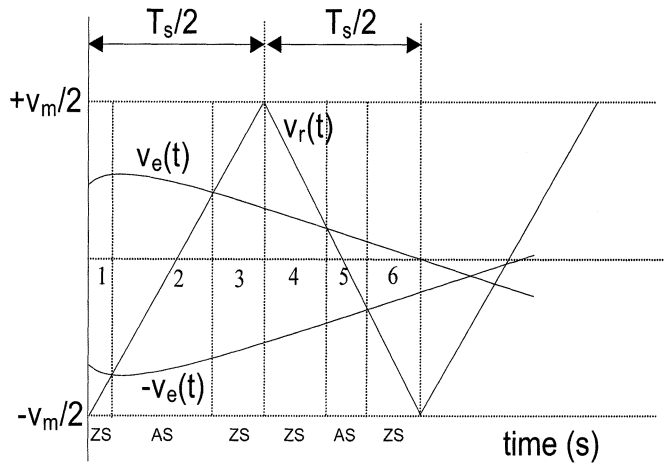

Fig. 2. Modulation scheme of the SPBBC involves four feasible switching states. Of these two are zero states (ZS), which occur when either the top or the bottom switches turn on simultaneously. The active states (AS) occur when either u_1 and u_4 or u_2 and u_3 turn on simultaneously.

is the nominal solution. This possibility is completely ignored in linearized averaged models. Consequently, the small-signal model can not predict the post-instability dynamics.

Using a switching model and a nonlinear map of a single-switch boost power-factor-correction circuit and Lyapunov's method and bifurcation analysis, Mazumder *et al.* [10] analyzed the stability and dynamics of the converter in the saturated and unsaturated regions. This methodology overcomes the three deficiencies of linearized averaged models. The new approach predicts not only the instabilities, but also the mechanism of these instabilities; knowledge of the latter can lead to effective bifurcation controllers. In this paper, we extend the methodology described in [10] to analyze the stability of a SPBBC, operating in the continuous-conduction mode (CCM) and in the unsaturated region. We show that the instability in such a converter can occur on slow and fast scales. Furthermore, we describe the mechanism of these instabilities.

II. Analytical Map of a Single-Phase-Bidirectional-Boost Converter

Fig. 1 shows a single phase bidirectional boost converter [19]. We assume that all of the switches of the SPBBC are ideal. The status of the four switches at any instant defines a switching state. For the bidirectional converter, 16 switching states are possible. However, only four of these are feasible for the SPBBC. Two of these states are zero states (ZS); the other two are the active states (AS). As shown in Fig. 2, the four switching states of the SPBBC are generated by comparing the error signals $v_{e1}(t)$ and $-v_{e1}(t)$ with a triangular carrier waveform $v_r(t)$ of frequency $f_s(= \omega_s/2\pi = 1/T_s)$. The present methodology holds also holds for case in which the carrier waveform is different from the one shown in Fig. 2.

The dynamical equation of the converter in the i^{th} sub-interval (of duration δ_i) of the k^{th} switching cycle is described by

$$\dot{X}(t) = A_i X(t) + B_i v_{in}(t) \tag{1}$$

where the A_i and B_i are matrices, $X(t) = [i_L(t)\ v_C(t)]^T$ represents the states of the converter, and $v_{in}(t)$ is a time-varying input voltage. The matrices A_i and B_i are obtained from the vector-differential equation describing $\dot{i}_L(t)$ and $\dot{v}_C(t)$ for a given switching state. The solution of (1) is given by

$$X(t) = e^{\int_{t_0}^{t} A_i d\tau} X(t_0) + \int_{t_0}^{t} e^{\int_{\tau}^{t} A_i d\xi} B_i v_{in}(\tau) d\tau \tag{2}$$

where t_0 is the initial time. By cascading the solutions of (2) over all of the subintervals of the k^{th}-switching cycle, we obtain a first-order Poincare map for the SPBBC. Next, we assume that the forcing function is given by

$$v_{in}(t) = v_m \cos(\omega_l t) \tag{3}$$

where v_m and ω_l are the amplitude and frequency of $v_{in}(t)$. Such an assumption is quite close to reality for most of the practical cases and has been used in many earlier papers [1], [5]–[9], [18]. Using (2) and (3) and some algebra, one can show that the map, which describes the dynamics of the SPBBC, in the i^{th} sub-switching cycle (of duration δ_i) of the k^{th} switching cycle is given by [19]

$$\begin{aligned} X(k+i+1) = {} & e^{A_i\delta_i} X(k+i) + \frac{e^{j\omega_l\delta_i}}{2} v_m M_i \left(e^{(J_i - j\omega_l I)\delta_i} - I\right) \\ & \times (J_i - j\omega_l I\delta_i)^{-1} M_i^{-1} B_i + \frac{e^{-j\omega_l\delta_i}}{2} v_m M_i \\ & \times \left(e^{(J_i + j\omega_l I)\delta_i} + I\right)(J_i + j\omega_l I\delta_i)^{-1} M_i^{-1} B_i \end{aligned} \tag{4}$$

where J_i and M_i are the Jordan and modal matrices of A_i, I is the identity matrix, and j is a complex operator. Although (4) looks like a map in complex space, a manipulation would show that it is actually real.

Special case ($\omega_l = 0$): When $\omega_l = 0$, using the relation $A_i = M_i^{-1} J_i M_i$, (4) reduces to

$$X(k+i+1) = e^{A_i\delta_i} X(k+i) + (e^{A_i\delta_i} - I) A_i^{-1} B_i v_m \tag{5}$$

which is the expression we obtained for a dc-dc converter in a sub-switching cycle [14], [15]. This confirms that (4) is a general map, which can be used for ac-dc as well as dc-dc converters. The methodology to prove the existence of the first-order Poincare map for a single-phase boost converter is described in [10].

Using (4), we obtain the solutions in all of the sub-intervals of the k^{th} switching cycle, and by cascading all of these solutions, one can obtain a map that relates X_{k+1} to X_k. Such a map has the form

$$X(k+1) = f\left(X(k), t_1(k), t_2(k), \cdots, t_6(k)\right) \tag{6}$$

and is referred to throughout the paper as the first-order Poincare map of the SPBBC. In (6), $t_1(k), t_2(k), \cdots, t_6(k)$ represent the time duration of each subswitching cycle in a switching cycle of period T_s.

If $v_{in}(t)$ has finite (N) higher-order harmonics and is described by

$$v_{in}(t) = \Sigma_{p=1}^{N} v_{\alpha_p} \cos(p\omega_l t + \phi_{\alpha_p}) + \Sigma_{p=1}^{N} v_{\beta_p} \sin(p\omega_l t + \phi_{\beta_p}) \tag{7}$$

where v_{α_p} and v_{β_p} and are the amplitudes and ϕ_{α_p} and ϕ_{β_p} are the phases of the corresponding harmonics, then, the procedure

to obtain the solution of (2) is the same as that used to obtain (4), but it becomes more involved.

Another approach to obtain the solution of (1) when v_{in} has higher-order harmonics is as follows. Let

$$\begin{aligned} y_{\alpha_1}(t) &= \cos(\omega_l t + \phi_{\alpha_1}) \\ y_{\alpha_2}(t) &= \cos(2\omega_l t + \phi_{\alpha_2}) \\ &\vdots \\ y_{\alpha_N}(t) &= \cos(N\omega_l t + \phi_{\alpha_N}) \end{aligned} \tag{8}$$

and

$$\begin{aligned} y_{\beta_1}(t) &= \sin(\omega_l t + \phi_{\beta_1}) \\ y_{\beta_2}(t) &= \sin(2\omega_l t + \phi_{\beta_2}) \\ &\vdots \\ y_{\beta_N}(t) &= \sin(N\omega_l t + \phi_{\beta_N}) \end{aligned} \tag{9}$$

then using (8) and (9), one can rewrite (7) as

$$\begin{aligned} v_{in}(t) = {} & v_{\alpha_1} y_{\alpha_1}(t) + v_{\alpha_2} y_{\alpha_2}(t) + \cdots + v_{\alpha_N} y_{\alpha_N}(t) \\ & + v_{\beta_1} y_{\beta_1}(t) + v_{\beta_2} y_{\beta_2}(t) + \cdots + v_{\beta_N} y_{\beta_N}(t) \end{aligned} \tag{10}$$

where

$$\begin{aligned} \dot{y}_{\alpha_1}(t) &= y_{\alpha_{1a}}(t) = -\omega_l \sin(\omega_l t + \phi_{\alpha_1}) \\ \dot{y}_{\alpha_{1a}}(t) &= -\omega_l^2 \cos(\omega_l t + \phi_{\alpha_1}) = -\omega_l^2 y_{\alpha_1}(t) \\ \dot{y}_{\alpha_2}(t) &= y_{\alpha_{2a}}(t) = -2\omega_l \sin(2\omega_l t + \phi_{\alpha_2}) \\ \dot{y}_{\alpha_{2a}}(t) &= -4\omega_l^2 \cos(2\omega_l t + \phi_{\alpha_2}) = -4\omega_l^2 y_{\alpha_2}(t) \\ &\vdots \\ \dot{y}_{\alpha_N}(t) &= y_{\alpha_{Na}}(t) = -N\omega_l \sin(N\omega_l t + \phi_{\alpha_N}) \\ \dot{y}_{\alpha_{Na}}(t) &= -N^2\omega_l^2 \cos(N\omega_l t + \phi_{\alpha_N}) \\ &= -N^2\omega_l^2 y_{\alpha_N}(t) \end{aligned} \tag{11}$$

and

$$\begin{aligned} \dot{y}_{\beta_1}(t) &= y_{\beta_{1a}}(t) = \omega_l \cos(\omega_l t + \phi_{\beta_1}) \\ \dot{y}_{\beta_{1a}}(t) &= -\omega_l^2 \sin(\omega_l t + \phi_{\beta_1}) = -\omega_l^2 y_{\beta_1}(t) \\ \dot{y}_{\beta_2}(t) &= y_{\beta_{2a}}(t) = 2\omega_l \cos(2\omega_l t + \phi_{\beta_2}) \\ \dot{y}_{\beta_{2a}}(t) &= -4\omega_l^2 \sin(2\omega_l t + \phi_{\beta_2}) = -4\omega_l^2 y_{\beta_2}(t) \\ &\vdots \\ \dot{y}_{\beta_N}(t) &= y_{\beta_{Na}} = N\omega_l \cos(N\omega_l t + \phi_{\beta_N}) \\ \dot{y}_{\beta_{Na}}(t) &= -N^2\omega_l^2 \sin(N\omega_l t + \phi_{\beta_N}) \\ &= -N^2\omega_l^2 y_{\beta_N}(t). \end{aligned} \tag{12}$$

Thus, by using (8)–(12) instead of (3) and following the procedure described in [19], we obtain a first-order Poincare map by cascading the solution [described by (2)] for each of the six subintervals shown in Fig. 2. Overall, the procedures for obtaining (4) and (6) if $v_{in}(t)$ is described by (3) or (7) are similar.

Once a fist-order map is obtained, we use it to obtain a second-order Poincare map. Unlike a dc-dc converter, a second-order Poincare map may be necessary for the stability analysis of a SPBBC [19]. This is because, even under steady-state conditions, the output of the first-order Poincare map of a SPBBC, as described by (6), is time varying. A second-order Poincare map converts the problem from one of analyzing the stability of an orbit to that of analyzing the stability of a fixed point [20], [21]. Depending on the ratio of ω_l and ω_s, the second-order Poincare map is obtained as follows.

- (ω_s/ω_l) is an integer: In this case, the map is obtained by cascading (ω_s/ω_l) solutions of (6).
- ω_s and ω_l have a least common multiple (LCM): In this case, the map is obtained by cascading $(\omega_s/LCM(\omega_s,\omega_l))$ solutions of (6). For example, if $\omega_s = (2\pi)(10000)$ rad/sec and $\omega_l = (2\pi)(60)$ rad/sec, then $\mathrm{LCM}(\omega_s,\omega_l) = (2\pi)(20)$ rad/sec. The latter is often described as the mode-locked frequency [21].
- ω_s and ω_l have no common multiple: In this case, the map is obtained by interpolation [20].

The first two conditions are two specific cases of the final condition. While, the first two conditions are useful for obtaining the fixed points of the second-order Poincare map, one has to rely on linear interpolation for local stability analysis [20].

III. Analytical Map of a Closed-Loop Single Phase Bidirectional Boost Converter

Having modeled the open-loop converter, we extend the idea to model a closed-loop converter. We select a control such that the converter operates with unity power factor. There are many possible control laws; we select the one shown in Fig. 3 to demonstrate the modeling methodology. In Fig. 3, C is a row matrix and f_{vdc}, f_v, and f_i are the feedback-sensor gains for the output- and input-voltages and inductor current, respectively. Symbols ω_{iv} and ω_{pv} are the dc gain and pole frequency for the bus-voltage loop, which has a reference voltage of v_{ref}. Symbols ω_{ii} and ω_{pi} and ω_{zi} are the dc gain and pole and zero frequency for the inner current loop. The closed-loop states of the controllers are represented by ψ_3, ψ_4, and ψ_5. Switches u_1 and u_3 and u_2 and u_4 are complementary. As such and as explained in Section II, only two algebraic equations are sufficient for describing the modulator in Fig. 3.

Using (3), the idea described in (8)–(12), and Fig. 3, we obtain the following state-space model, which describes the dynamics of the converter for the i^{th} switching state

$$\begin{aligned} \dot{\Psi}(t) &= \begin{pmatrix} \dot{\psi}_1(t) \\ \dot{\psi}_2(t) \\ \dot{\psi}_3(t) \\ \dot{\psi}_4(t) \\ \dot{\psi}_5(t) \\ \dot{\psi}_6(t) \\ \dot{\psi}_7(t) \end{pmatrix} \\ &= \begin{pmatrix} c_{i_{11}} & c_{i_{12}} & 0 & 0 & 0 & c_{i_{16}} & c_{i_{17}} \\ c_{i_{21}} & c_{i_{22}} & 0 & 0 & 0 & 0 & 0 \\ c_{i_{31}} & c_{i_{32}} & c_{i_{33}} & 0 & 0 & 0 & 0 \\ c_{i_{41}} & 0 & c_{i_{43}}\psi_6(t) & 0 & 0 & 0 & 0 \\ c_{i_{51}} & 0 & c_{i_{53}}\psi_6(t) & c_{i_{54}} & c_{i_{55}} & 0 & 0 \\ 0 & 0 & 0 & 0 & 0 & 0 & 1 \\ 0 & 0 & 0 & 0 & 0 & c_{i_{76}} & 0 \end{pmatrix} \\ &\quad \times \begin{pmatrix} \psi_1(t) \\ \psi_2(t) \\ \psi_3(t) \\ \psi_4(t) \\ \psi_5(t) \\ \psi_6(t) \\ \psi_7(t) \end{pmatrix} + \begin{pmatrix} 0 \\ 0 \\ 1 \\ 0 \\ 0 \\ 0 \\ 0 \end{pmatrix} v_{ref}. \end{aligned} \tag{13}$$

In (13), $X(t) = (\psi_1(t) \quad \psi_2(t))^T$ and the $c_{i_{jk}}$ are coefficients, which can be easily obtained from the dynamical equations of the i^{th} topology. We note that, if instead of (3), we use the v_{in}

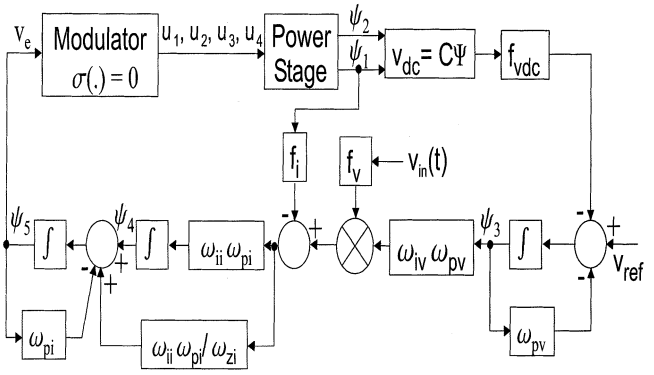

Fig. 3. Closed-loop controller for the SPBBC to achieve unity power-factor operation.

described by (7), then, as shown in Section II, the overall analysis for the closed-loop system remains the same but becomes more involved.

The solutions of $\psi_1(t)$, $\psi_2(t)$, $\psi_3(t)$, $\psi_6(t)$, and $\psi_7(t)$ in matrix form are

$$\begin{aligned}\Psi_a(t) &= (\psi_1(t)\psi_2(t)\psi_3(t)\psi_6(t)\psi_7(t))^T \\ &= e^{A_{a_i}t}\Psi_a(t_0) + \left(e^{A_{a_i}t} - I\right) A_{a_i}^{-1} B_{a_i} v_{ref} \\ &= M_{a_i} e^{J_{a_i}t} {M_{a_i}}^{-1} \Psi_a(t_0) \\ &\quad + \left(M_{a_i} e^{J_{a_i}t} {M_{a_i}}^{-1} - I\right) A_{a_i}^{-1} B_{a_i} v_{ref}. \end{aligned} \quad (14)$$

In (14), $\Psi_a(t) = (\psi_1(t)\psi_2(t)\psi_3(t)\psi_6(t)\psi_7(t))^T$ and J_{a_i} and M_{a_i} are the corresponding Jordan and modal matrices of A_{a_i}. We assume in (14) that Jordan decomposition of A_{a_i} is possible. This is based on following values of the power-stage parameters: $L = 5\ m\text{H}$, $r_L = 0.75\ \Omega$, $r_C = 0.5\ \Omega$, $C = 1000\ \mu\text{F}$, $f_{vdc} = 0.01$, $f_i = 0.1$, $\omega_{iv} = 35$, $\omega_{pv} = 2 \cdot \pi \cdot 15$ rad/s, $\omega_{ii} = 5 \cdot 10^4$, $\omega_{zi} = 2 \cdot \pi \cdot 950$ rad/s, $v_m = 110\sqrt{2}$ V, $\omega_s = 2\pi 10\,000$ rad/s, and $\omega_l = 2 \cdot \pi \cdot 60$ rad/s. In almost all of the practical cases, this assumption is true. Even if this assumption fails, the remaining procedure is the same but is more involved.

Letting

$$\underline{\Psi}_a(t) = M_{a_i}^{-1} \Psi_a(t) \quad (15)$$

and then substituting (15) into (14), we obtain

$$\begin{aligned}\underline{\Psi}_a(t) &= e^{J_{a_i}t}\underline{\Psi}_a(t_0) + \left(e^{J_{a_i}t} {M_{a_i}}^{-1} - M_{a_i}^{-1} I\right) A_{a_i}^{-1} B_{a_i} v_{ref} \\ &= e^{J_{a_i}t}\xi_0 + L_0 \end{aligned} \quad (16)$$

where

$$\begin{aligned}\xi_0 &= (\xi_{10}\ \xi_{20}\ \xi_{30}\ \xi_{60}\ \xi_{70})^T \\ &= \underline{\Psi_a}(t_0) + {M_{a_i}}^{-1} {A_{a_i}}^{-1} B_{a_i} v_{ref} \\ L_0 &= (L_{10}\ L_{20}\ L_{30}\ L_{60}\ L_{70})^T \\ &= -{M_{a_i}}^{-1} I {A_{a_i}}^{-1} B_{a_i} v_{ref}. \end{aligned} \quad (17)$$

Using (13)–(15), we rewrite $\dot{\psi}_4(t)$ as

$$\dot{\psi}_4(t) = P_{1a_i} M_{a_i} \underline{\Psi}_a(t) + P_{6a_i} M_{a_i} \underline{\Psi}_a(t) P_{3a_i} M_{a_i} \underline{\Psi}_a(t) \quad (18)$$

where $P_{1a_i} = (c_{i_{41}} 0\ 0\ 0\ 0\ 0)$, $P_{3a_i} = (0\ 0\ c_{i_{43}}\ 0\ 0\ 0)$, and $P_{6a_i} = (0\ 0\ 0\ 0\ 0\ 1)$. Solving (18) yields

$$\psi_4(t) = \psi_4(t_0) + \int_{t_0}^{t} g(\tau) d\tau. \quad (19)$$

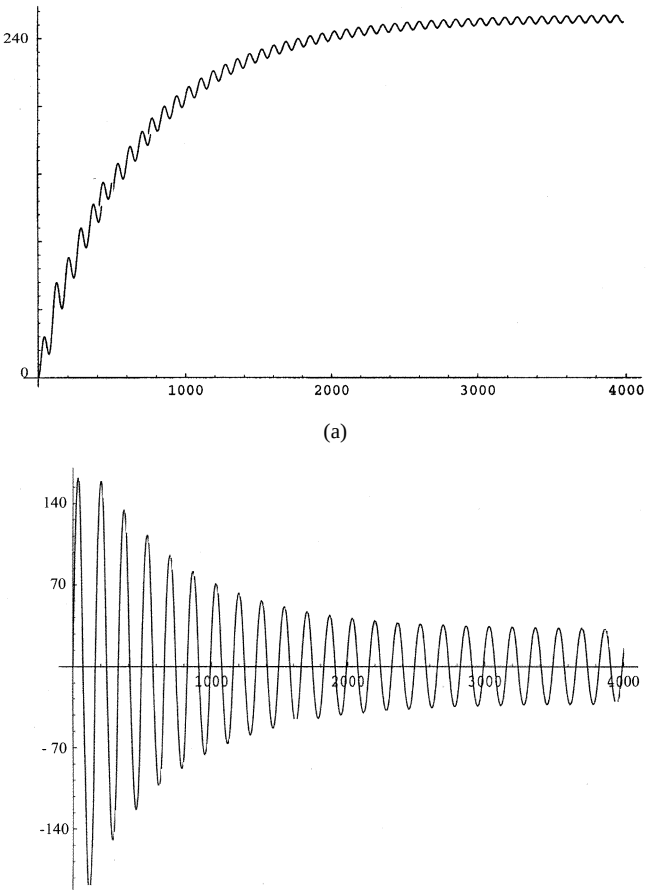

Fig. 4. Open-loop response of the SPBBC: (a) capacitor voltage in volts and (b) inductor current in amperes. The horizontal axes for both plots represent the number of switching cycles.

where

$$\begin{aligned} g(\tau) &= P_{1a_i} M_{a_i} \underline{\Psi}_a(\tau) \\ &\quad + P_{6a_i} M_{a_i} \underline{\Psi}_a(\tau) P_{3a_i} M_{a_i} \underline{\Psi}_a(\tau). \end{aligned} \quad (20)$$

Using (16) and (20), one can show that all of the integral terms in (19) except for one can be determined exactly in matrix form. The exact solution of the latter is found by integrating its individual elements. Once $\psi_4(t)$ is obtained, the solution of $\psi_5(t)$ is obtained in a similar manner. Thus, we have an analytical solution for $\Psi(t)$ in the i^{th} switching cycle. The procedure to obtain the first- and second-order Poincare map using the solution of the closed-loop states $\Psi(t)$ is the same as that described in Section II.

IV. Results

Fig. 4 shows the behavior of the open-loop SPBBC during startup obtained using the first-order Poincare map described by (6). The error signal v_e, which determines the duration of the zero and active states, is predetermined such that at steady state the average of the bus voltage is 245 V. It takes about 4000 iterations to achieve the steady state. Using the analytical map, the entire simulation is completed in about 2 min. Using ideal

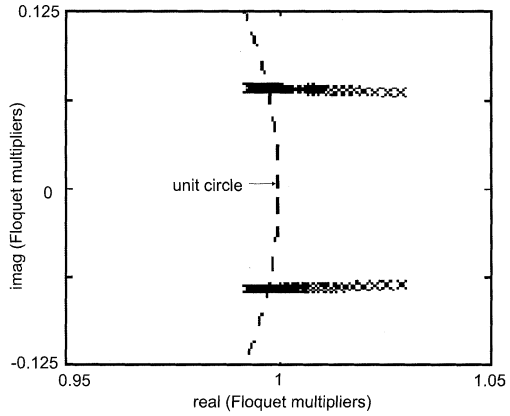

Fig. 5. As the current-loop controller gain ω_{iv} is gradually increased, two of the Floquet multipliers exit the unit circle as complex conjugates, which indicates a Hopf bifurcation. This leads to an instability on the slow scale.

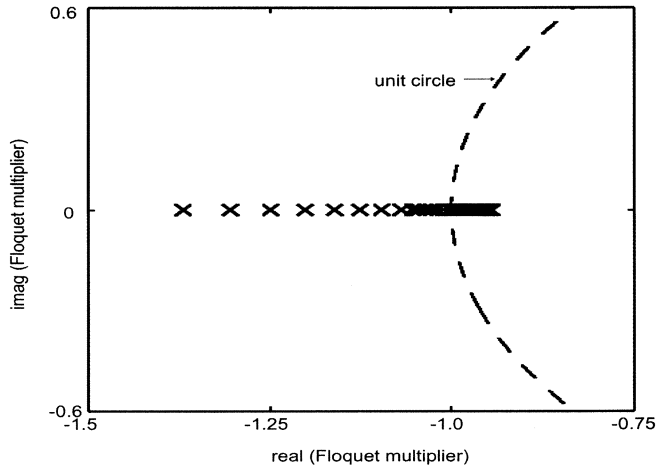

(a)

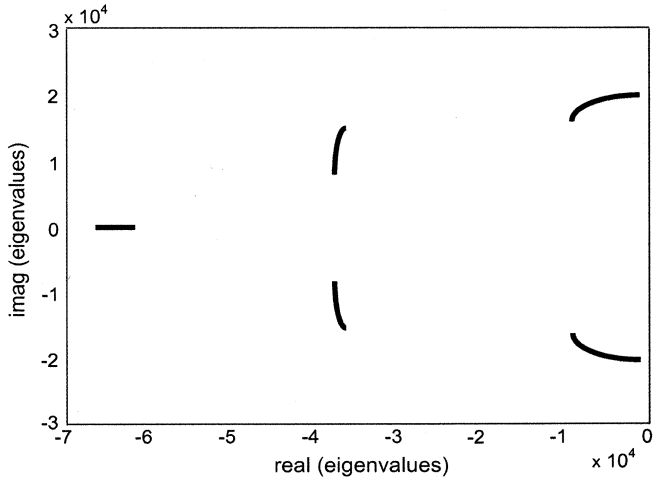

(b)

Fig. 6. (a) As the current-loop controller gain ω_{ii} is gradually increased, one of the Floquet multipliers of the map exits the unit circle via -1, which indicates a period-doubling bifurcation. This leads to an instability on the fast scale. (b) The eigenvalues of the averaged model show a stable system because the averaged model can not account for the switching-frequency dynamics.

switches, a standard simulator, like Saber, running on the same machine took over 60 min to complete the same simulation.

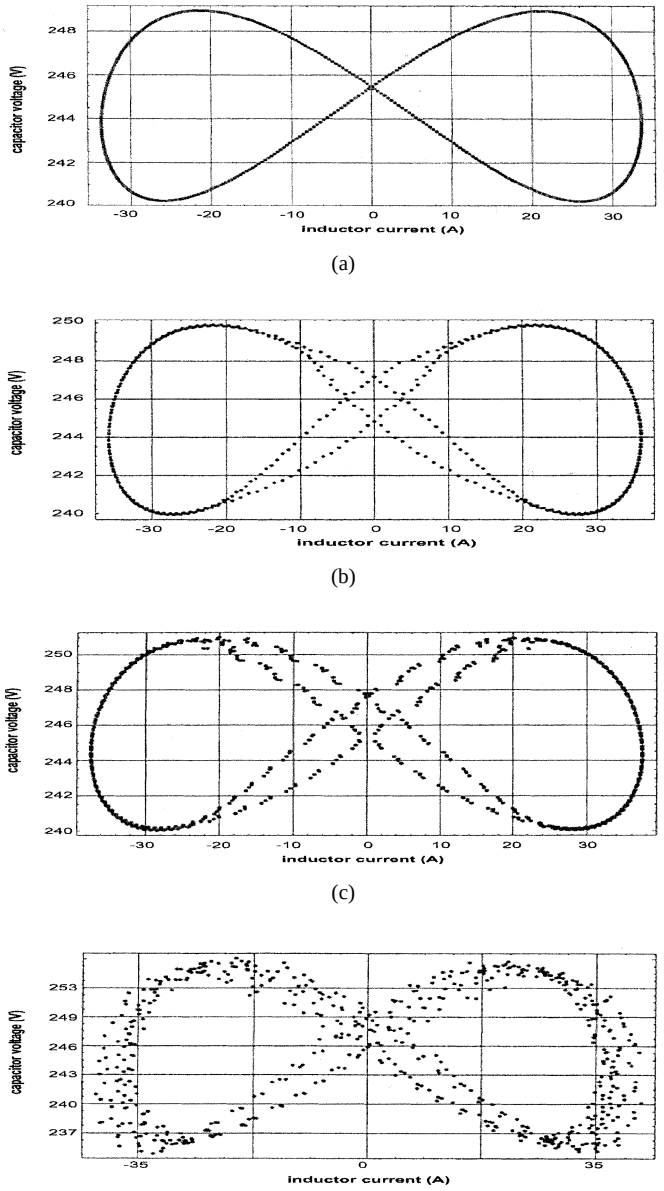

(a)

(b)

(c)

(d)

Fig. 7. Impact of variations in ω_{ii} on the stability of the bidirectional converter: (a) stable system, (b) a period-doubling bifurcation results in fast-scale instability, and (c) and (d) increasing the value of the bifurcation parameter (ω_{ii}) ultimately leads to chaos.

Next, we investigate the dynamics of the closed-loop SPBBC, which operates as a power-factor correction circuit and in continuous-conduction mode (CCM). Using the shooting method [21], we trace the Floquet multipliers [21] of the second-order map of the SPBBC as the voltage-loop controller gain (ω_{iv}) is gradually increased from its nominal value. For stability, all of the Floquet multipliers should be within the unit circle [21]. Fig. 5 shows the impact of variations in ω_{iv} on the stability of the SPBBC. It shows that as ω_{iv} is gradually increased, two of the Floquet multipliers leave the unit circle away from the real axis, indicating a Hopf bifurcation [21]. This results in a slow scale instability, which can be predicted using an averaged model of the SPBBC [22].

Fig. 6(a) shows the impact of variations in ω_{ii} (dc gain) on the stability of the SPBBC. As the controller gain is gradually

increased, one of the Floquet multipliers exits the unit circle via -1 indicating a period-doubling bifurcation. The Poincare maps in Fig. 7 show that as the gain is increased, the system which is initially stable [Fig. 7(a)], undergoes a torus breakdown via a period-doubling bifurcation [Fig. 7(b)], which ultimately leads to chaos [Fig. 7(d)]. Physically, with progressively higher gain, a new order is established for the ripple dynamics while the average dynamics remains the same. This type of instability, which occurs on the fast scale [14]–[16], can not be predicted by an averaged model of the SPBBC [14]–[16], [22]. Fig. 6(b) confirms this prediction. It shows that, for the same variation in ω_{ii} used to obtain Fig. 6(a), all of the eigenvalues of the linearized averaged model of the SPBBC are in the left-half plane; it indicates a stable system [21].

V. Conclusion

We modeled an open- and closed-loop single-phase-bidirectional boost converter using a second-order Poincare map, which converts the problem from one of analyzing a nonsmooth system to a smooth system. The analytical map enables the analysis of the dynamics of the system much faster and without convergence problems. For the closed-loop system, using the nonlinear map, we investigated the slow- and fast-scale instabilities of the converter. The slow-scale instability occurs due to a Hopf bifurcation. Such an instability can also be predicted by averaged models [22]. The fast-scale instability occurs due to a period-doubling bifurcation. The fast-scale instability leads to a torus breakdown and ultimately the converter enters a chaotic state. This kind of instability can not be predicted by averaged models [14]–[16], [19] because they do not account for the switching-frequency dynamics.

References

[1] N. Mohan, T. M. Undeland, and R. J. Ferraro, "Sinusoidal line current rectification with a 100 kHz B-SIT step-up converter," in *Proc. IEEE Power Electron. Spec. Conf.*, 1984, pp. 92–98.

[2] C. P. Henze and N. Mohan, "A digitally controlled ac to dc power conditioner that draws sinusoidal input current," in *Proc. IEEE Power Electron. Spec. Conf.*, 1986, pp. 531–540.

[3] J. B. Williams, "Design of feedback loop in unity power factor ac to dc converter," in *Proc. IEEE Power Electron. Spec. Conf.*, 1989, pp. 959–967.

[4] P. Todd, UC3854 Controlled power factor correction circuit design, Tech. Rep., Unitrode, Inc., 1999.

[5] C. Zhou, R. B. Ridley, and F. C. Lee, "Design and analysis of a hysteretic boost power factor correction circuit," in *Proc. IEEE Power Electron. Spec. Conf.*, 1990, pp. 800–807.

[6] C. Zhou and M. M. Jovanović, "Design trade-offs in continuous current-mode controlled boost power factor correction circuits," in *Proc. High-Freq. Power Conv. Conf.*, 1992, pp. 209–220.

[7] R. B. Ridley, "Average small-signal analysis of the boost power factor correction circuit," in *Proc. Virginia Power Electron. Center Sem.*, 1989, pp. 108–120.

[8] F. A. Huliehel, F. C. Lee, and B. H. Cho, "Small-signal modeling of the single-phase boost high factor converter with constant frequency control," in *Proc. IEEE Power Electron. Spec. Conf.*, 1992, pp. 475–482.

[9] D. Simonetti, J. Sebastiań, J. A. Cobos, and J. Uceda, "The continuous-discontinuous conduction boundary of a boost PFP fed by universal input," in *Proc. CIEP*, 1995, pp. 20–24.

[10] S. K. Mazumder and A. H. Nayfeh, "A new approach to the stability analysis of boost power-factor-correction circuits," *J. Vibr. Contr.*, to be published.

[11] S. R. Sanders, J. M. Noworolski, X. J. Liu, and G. C. Verghese, "Generalized averaging method for power conversion circuits," *IEEE Trans. Power Electron.*, vol. 6, pp. 251–259, Mar. 1991.

[12] A. M. Stankovic, S. R. Sanders, and T. Aydin, "Analysis of unbalanced ac machines with dynamic phasors," in *Proc. Naval Symp. Electric Machines*, 1998, pp. 219–224.

[13] C. B. Jacobina, M. B. R. Correa, T. M. Oliveira, A. M. Lima, and E. R. C. da Silva, "Vector modeling and control of unbalanced electrical systems," in *Proc. IEEE Ind. Applicat. Soc.*, 1999, pp. 1011–1017.

[14] M. Alfayyoumi, A. H. Nayfeh, and D. D. Boroyevich, "Modeling and analysis of switching-mode dc-dc regulators," *Int. J. Bifurcation Chaos*, vol. 10, no. 2, pp. 373–390, 2000.

[15] S. K. Mazumder, A. H. Nayfeh, and D. Boroyevich, "Theoretical and experimental investigation of the fast- and slow-scale instabilities of a dc-dc converter," *IEEE Trans. Power Electron.*, vol. 16, pp. 201–216, Mar. 2001.

[16] ——, "Nonlinear dynamics and stability analysis of parallel dc-dc converters," in *Proc. IEEE Power Electron. Spec. Conf.*, 2001, pp. 1283–1288.

[17] R. W. Erickson, S. Ćuk, and R. D. Middlebrook, "Large-signal modeling and analysis of switching regulators," in *Proc. IEEE Power Electron. Spec. Conf.*, 1982, pp. 240–250.

[18] S. Hiti, "Modeling and control of three-phase PWM converters," Ph.D. dissertation, Dept. Elect. Comput. Eng., Virginia Polytech.c Inst. State Univ., Blacksburg, Virginia, 1995.

[19] S. K. Mazumder, "Nonlinear analysis and control of standalone, parallel dc-dc, and parallel multi-phase PWM converters," Ph.D. Dissertation, Dept. Elect. Comput. Eng., Virginia Polytech.c Inst. State Univ., Blacksburg, VA, 2001.

[20] C. Kaas-Petersen, "Computation of quasiperiodic solutions of forced dissipative systems," *J. Computat. Phys.*, vol. 58, pp. 395–408, 1986.

[21] A. H. Nayfeh and B. Balachandran, *Applied Nonlinear Dynamics*. New York: Wiley, 1995.

[22] S. Chandrasekaran, "Optimization tools for subsystem design in aircraft power distribution systems," Ph.D. dissertation, Dept. Elect. Comput. Eng., Virginia Polytech.c Inst. State Univ., Blacksburg, VA, 2000.

[23] R. M. Bass and J. Sun, "Large-signal averaging methods under large ripple conditions (for power convertors)," in *Proc. IEEE Power Electron. Spec. Conf.*, 1998, pp. 630–632.

[24] R. M. Bass and B. Lehman, "Switching frequency dependent averaged models for PWM dc-dc converters," *IEEE Trans. Power Electron.*, vol. 11, pp. 89–98, Jan. 1996.

[25] D. C. Hamill, J. H. B. Deane, and D. J. Jefferies, "Modeling of chaotic dc-dc converters by iterated nonlinear mappings," *IEEE Trans. Power Electron.*, vol. 7, pp. 25–36, Jan. 1992.

[26] C. K. Tse, "Flip bifurcation and chaos in three-state boost switching regulators," *IEEE Trans. Circuits Syst. I*, vol. 41, pp. 16–23, Jan. 1994.

[27] ——, "Chaos from a buck switching regulator operating in the discontinuous mode," *Int. J. Circuit Theory Applicat.*, vol. 22, pp. 263–278, 1994.

[28] E. Fossas and G. Olivar, "Study of chaos in the buck converter," *IEEE Trans. Circuits Syst. I*, vol. 43, pp. 13–25, Jan. 1996.

[29] M. diBernardo, E. Fossas, G. Olivar, and F. Vasca, "Secondary bifurcations and high periodic orbits in voltage controlled buck converter," *Int. J. Bifurcation Chaos*, vol. 7, pp. 2755–2771, 1997.

[30] G. H. Yuan, S. Bannerjee, E. Ott, and J. A. Yorke, "Border collision bifurcations in the buck converter," *IEEE Trans. Circuits Syst. I*, vol. 45, pp. 707–716, July 1998.

[31] A. ElAroudi, G. Olivar, L. Benadero, and E. Toribio, "Hopf bifurcation and chaos from torus breakdown in a (PWM) voltage-controlled dc-dc boost converter," *IEEE Trans. Circuits Syst. I*, vol. 11, pp. 1374–1382, 1999.

[32] F. Gordillo, G. Escobar, and J. Aracil, "Bifurcation analysis of a power factor precompensator," in *Stability and Stabilization of Nonlinear Systems*, D. Aeyels, F. Lamnabhi-Lagarrigue, and A. J. van der Schaft, Eds. New York: Springer-Verlag, 1999, Lecture Notes in Control and Information Sciences, pp. 151–164.

[33] A. ElAroudi, L. Benadero, E. Toribio, and S. Machiche, "Quasiperiodicity and chaos in the dc-dc buck-boost converter," *Int. J. Bifurcation Chaos*, vol. 10, pp. 359–371, 2000.

[34] S. Banerjee, P. Ranjan, and C. Grebogi, "Bifurcation in two-dimension piecewise smooth maps—theory and applications in switching circuits," *IEEE Trans. Circuits Syst. I*, vol. 47, pp. 633–647, 2000.

[35] M. diBernardo and F. Vasca, "Discrete-time maps for the analysis of bifurcations and chaos in dc/dc converters," *IEEE Trans. Circuits Syst. I*, vol. 47, pp. 130–143, Feb. 2000.

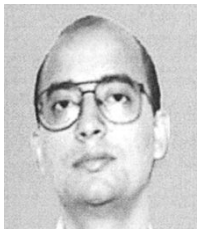

Sudip K. Mazumder (M'01) received the M.S. degree in electrical power engineering from the Rensselaer Polytechnic Institute (RPI), Troy, NY, in 1993 and the Ph.D. degree in electrical and computer engineering from the Virginia Polytechnic Institute and State University (VPI&SU), Blacksburg, VA, in 2001.

He is currently an Assistant Professor at the Power Electronics Research Center (PERC), Department of Electrical and Computer Engineering, University of Illionoic, Chicago. He has over 10 years of experience and has held R&D and design positions in leading industrial organizations. he has published over 35 refereed and invited journal and conference papers and is a Reviewer for six international journals. His areas of expertise and interest include interactive power/power-electronic networks (IPNs), renewable/alternative energy systems and distributed generation, optical switching in power electronics, wireless motion sensing and wide-area power management, advanced control and DSP/RISC and ASIC-based embedded controllers for power supplies/systems and motor drives, power quality and voltage sags, soft-switching and hard-switching topologies and techniques in power converters, and packaging.

Dr. Mazumder received the DOE SECA Award in 2002, the NSF CAREER Award in 2003, and the Prize Paper Award from the IEEE TRANSACTIONS ON POWER ELECTRONICS and the IEEE Power Electronics Society, in 2002, and the Solid-State Energy Conversion Alliance (SECA) Award from the Department of Energy in 2002. He is listed in *Who's Who in Engineering Education*. He is an Associate Editor of the IEEE TRANSACTIONS ON INDUSTRIAL ELECTRONICS and the IEEE POWER ELECTRONICS LETTERS.

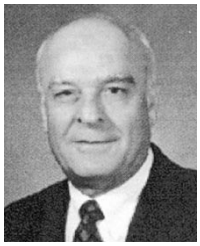

Ali H. Nayfeh was born in Shuwaikah, Jordan, on December 21, 1933. He received the B.S. degree in engineering science and the M.S. and Ph.D. degrees in aeronautics and astronautics from Stanford University, Stanford, CA, in 1962, 1963, and 1964, respectively.

He has industrial experience with Heliodyne Corporation and Aerotherm Corporation. He is the author of the Wiley-Interscience books *Perturbation Methods*, *Introduction to Perturbation Techniques*, *Problems in Perturbation*, *Method of Normal Forms*, and *Nonlinear Interactions* (Wiley-Interscience) and coauthor of *Nonlinear Oscillations*, *Applied Nonlinear Dynamics*, *Perturbation Methods with Maple*, and *Perturbation Methods with Mathematics* (Wiley-Interscience). He is the Editor of the Wiley Book Series *Nonlinear Science* and the Editor-in-Chief of *Nonlinear Dynamics* and the *Journal of Vibration and Control*. He established and served as Dean of the College of Engineering, Yarmouk University, Jordan from 1980–1984. He is currently University Distinguished Professor of Engineering at Virginia Polytechnic Institute and State University.

Dr. Nayfeh received the Kuwait Prize in Basic Sciences (Physics), in 1981, the American Institute of Aeronautics and Astronautics Pendray Aerospace Literature Award, in 1995, the American Society of Mechanical Engineers J. P. Den Hartog Award, in 1997, the Honorary Doctorate, St. Petersburg University, Russia, in 1996, the Frank J. Maher Award for Excellence in Engineering Education, in 1997, the College of Engineering Dean's Award for Excellence in Research, in 1998, and the Honorary Doctorate from the Technical University of Munchen, Germany, in 1999. He is a Fellow of the American Physical Society, the American Institute of Aeronautics and Astronautics, the American Society of Mechanical Engineers, and the American Academy of Mechanics.

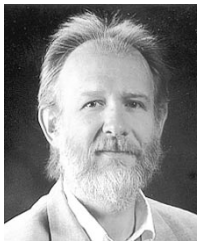

Dushan Boroyevich (M'85) received the Dipl.Ing. degree from the University of Belgrade, Yugoslavia, in 1976, the M. S. degree from the University of Novi Sad, Yugoslavia, in 1982, and the Ph.D. degree from the Virginia Polytechnic Institute and State University (Virginia Tech), Blacksburg, in 1986.

Between 1986 and 1990, he was an Assistant Professor and Director of the Power and Industrial Electronics Research Program, Institute for Power and Electronic Engineering, University of Novi Sad, and later, Acting Head of the Institute. In 1990, he joined The Bradley Department of Electrical and Computer Engineering, Virginia Tech, as Associate Professor. From 1996 to 1998, he was Associate Director of the Virginia Power Electronics Center, and since 1998 he has been the Deputy Director of the NSF Engineering Research Center for Power Electronics Systems and Professor at the Department. His research interests include multiphase power conversion, high-power PWM converters, modeling and control of power converters, applied digital control, and multidisciplinary modeling and design of integrated power modules. He has published over 100 technical papers, has three patents, and has been involved in numerous government and industry-sponsored projects in the areas of power and industrial electronics.